Computational analysis of electron transfer kinetics for CO_2 reduction with organic photoredox catalysts

Kareesa J. Kron,[†] Samantha J. Gomez,[†,‡] Robert J. Cave,[¶] and Shaama Mallikarjun Sharada[*,†,§]

†*Mork Family Department of Chemical Engineering and Materials Science, University of Southern California, Los Angeles, California, 90089, United States*

‡*Bravo Medical Magnet High School, Los Angeles, California, 90033, United States*

¶*Department of Chemistry, Harvey Mudd College, Claremont, California, 91711, United States*

§*Department of Chemistry, University of Southern California, Los Angeles, California, 90089, United States*

E-mail: ssharada@usc.edu

Abstract

We present a fundamental description of the electron transfer (ET) step from substituted oligo(p-phenylene) (OPP) radical anions to CO_2, with the larger goal of assessing the viability of underexplored, organic photoredox routes for utilization of anthropogenic CO_2. This work varies the electrophilicity of para-substituents to OPP and probes the dependence of rate coefficients and interfragment interactions on the substituent Hammett parameter, σ_p, using constrained density functional theory (CDFT) and energy decomposition analysis (EDA). Large electronic coupling elements across

substituents indicate an adiabatic electron transfer process for reactants at contact. As one might intuitively expect, free energy changes dominate trends in ET rate coefficients in most cases, and rates increase with substituent electron-donating ability. However, we observe an unexpected dip in rate coefficients for the most electron-donating groups, due to the combined impact of flattening free energies and a steep increase in reorganization energies. Our analysis shows that flattening OPP LUMO levels lower the marginal increase in free energy with decreasing σ_p. Reorganization energies do not exhibit a direct dependence on σ_p. They are higher for substituents containing lone pairs of electrons since substituent orientation varies with OPP charge. EDA reveals that interfragment orbital relaxation, or charge transfer interaction, plays a critical role in stabilizing the vertically excited charge transfer state. Subsequent relaxation to the final state geometry lowers charge transfer stabilization. A concurrent increase in long-range electrostatic interactions is observed, which are more favorable for electron-withdrawing substituents. Our study therefore suggests that while a wide range of ET rates are observed, there is an upper limit to rate enhancements achievable by tuning substituent electrophilicity.

Introduction

There is a pressing need today to combat rising levels of anthropogenic carbon dioxide owing to its detrimental impact on climate and the environment.[1] Light-driven chemistry with photoredox catalysts opens up sustainable, less energy-intensive routes towards utilization of CO_2 via conversion into useful precursors and products. Recent years have witnessed significant progress in the development of metal-based photocatalysts for CO_2 reduction.[2–7] Metal-free, organic catalytic routes for CO_2 utilization, on the other hand, are less explored even though they have the potential for lower environmental risk relative to their transition metal counterparts,[8,9] in addition to structural flexibility and tunability.[10–12] Organic photoredox catalysts utilize visible or ultraviolet light to access excited states. These excited

states are subsequently quenched to create highly reactive radical species that are capable of carrying out otherwise thermally demanding chemical transformations.[10,13–16]

Oligo(p-phenylenes) (OPPs) were first proposed as promising candidates for photoredox reduction of CO_2 in 1992 by Matsuoka and coworkers.[17] More recently, studies demonstrated amino acid synthesis and styrene hydrocarboxylation from CO_2 using OPPs.[18,19] Owing to their potential applications in areas besides catalysis including photoactive materials such as organic light-emitting diodes, the excited state properties of OPPs are well-characterized.[20–27] Several studies also probe the sensitivity of OPP excitations to torsional changes, chain length, and isomeric forms.[20,23,28] However, fundamental computational studies of electron transfer (ET) from excited states or quenched radicals are largely restricted to intramolecular processes for semiconductor applications.[29,30] This work therefore aims to determine driving forces for ET from OPP to CO_2 and utilize the outcomes to identify structural modifications necessary for achieving rate enhancements.

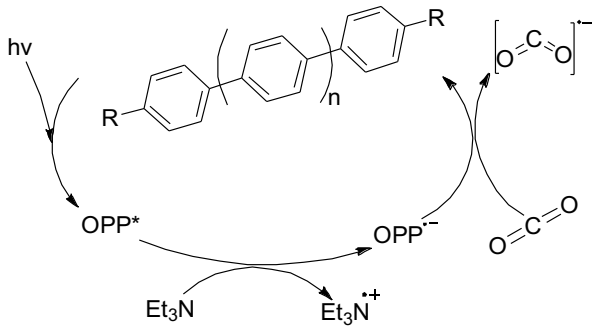

Figure 1: Proposed photoredox catalytic cycle – OPPs are excited by UV/Vis light (>290nm) and subsequently reduced to radical anions by a sacrificial electron donor such as triethylamine. CO_2 reduction by the anion regenerates OPP.[31]

The ET mechanism is based on the catalytic cycle proposed by Wada and coworkers, shown in Figure 1.[31] OPP forms an excited state singlet, OPP*, upon absorbing light. This excited state is quenched to create a radical anion using a sacrificial donor such as triethylamine, Et_3N. The radical anion is highly reducing and therefore capable of initiating reduction of CO_2 by transferring an electron. This ET step also serves to regenerate OPP.

Experimental studies further report sensitivity of reaction rates and yields to oligomer chain length, choice of solvent, and added cations.[17,31]

Our objective is to probe driving forces for the ET step that reduces CO_2 by tuning the electron density of terphenyl (OPP with 3 phenyl rings) through the addition of terminal substituents of varying electrophilicity. This work is along similar lines to a recent study of ET properties of pyrene-based photocatalysts.[32] We utilize constrained density functional theory (CDFT)[33] to calculate rate coefficients for ET and energy decomposition analysis (EDA)[34] to characterize interactions between the catalyst and substrate fragments during key stages of ET. Physical intuition dictates that increasing substituent electron-donating character decreases the reduction potential of the resulting radical anion (in other words, the reaction free energy becomes more negative) and therefore increases ET rates. While we show that this is generally true, free energies plateau beyond a Hammett parameter (σ_p) of -0.75, a consequence of flattening OPP LUMO levels. Further, an unexpected reduction in ET rates is observed for strongly electron-donating groups, stemming from an increase in reorganization energies. Free energies can be correlated directly to substituent Hammett parameter. On the other hand, reorganization energies are impacted by torsional rotations of substituents, with larger values observed for substituents containing lone pairs of electrons. We utilize EDA to understand both free energies and reorganization energies from the perspective of catalyst-substrate interactions that constitute initial, final, and vertically excited charge transfer (VCT) states. While the fragments interact only weakly in the initial states, charge transfer (or interfragment relaxation) and electrostatics govern interfragment interaction differences across substituents in the VCT and final states, respectively. This analysis therefore demonstrates that while ET rates can be tuned using substituent electrophilicity, trends are not monotonic due to a combination of factors, not all of which are determined by electrophilicity.

Methods

All DFT[35,36] simulations are carried out using the *ab initio* quantum chemistry software, Q-Chem 5.2.1.[37] Terphenyl (OPP) with 20 distinct substituents of varying electrophilicity are chosen as model systems to calculate ET rates. Terphenyl is chosen as the representative OPP since it does not suffer from solubility issues observed with longer chains.[17] All calculations are carried out at the B3LYP/6-311G** level of theory[38] along with the polarizable continuum model (PCM)[39–41] to represent the solvation environment of CH_2Cl_2 (dielectric = 8.93, optical dielectric = 2.02834). Dispersion effects are captured using Grimme's D3 correction with Becke-Johnson (BJ) damping (D3-BJ).[42,43] The choice of level of theory is guided by benchmarking time-dependent DFT (TDDFT)[44,45] excitation energies with prior experiments and theory (Table 1, Supporting Information, SI).[20,46]

In the limit of weak interactions, the electron transfer rate is calculated using the non-adiabatic limit by Marcus:[47]

$$k = \sqrt{\frac{\pi}{\lambda k_B T}}\left(\frac{J^2}{\hbar}\right)e^{-\frac{\Delta G^*}{k_B T}} \tag{1}$$

where k_B is Boltzmann's constant, temperature T is 298.15 K to simulate experimental conditions,[17] $\hbar$ is Planck's constant, and λ is reorganization energy. J is the charge coupling constant, also known as the charge transfer integral or diabatic coupling. J is calculated using Configuration Interaction with CDFT (CDFT-CI) based on the initial state geometry.[48] We find (*vida infra*) that calculated J values are large, indicating that ET is adiabatic. Therefore, instead of Marcus Theory, we utilize the rate coefficient expression for adiabatic ET proposed by Brunschwig and coworkers:[49]

$$k = \nu e^{-\frac{\Delta G^*}{RT}} \tag{2}$$

ν is a weighted average of vibrational frequencies for modes that contribute to the reaction coordinate, usually approximated as 10^{13} sec^{-1}. Since we probe substituent effects, we calculate relative rates with unsubstituted OPP (denoted by subscript H) as reference, k/k_H.

The ET barrier, ΔG^*, is given by

$$\Delta G^* = \frac{\lambda}{4}\left(1 + \frac{\Delta G}{\lambda}\right)^2 \tag{3}$$

ΔG is the free energy change associated with the ET reaction step. ΔG and λ are calculated using CDFT based on the energy profile depicted in Figure 2. CDFT[33] is utilized to calculate energies of

- Initial state: $OPP^{\cdot -} + CO_2$
- Final state: $OPP + CO_2^{\cdot -}$
- Vertically excited charge transfer or VCT state: Electron is transferred to CO_2 but geometry is still that of the initial state

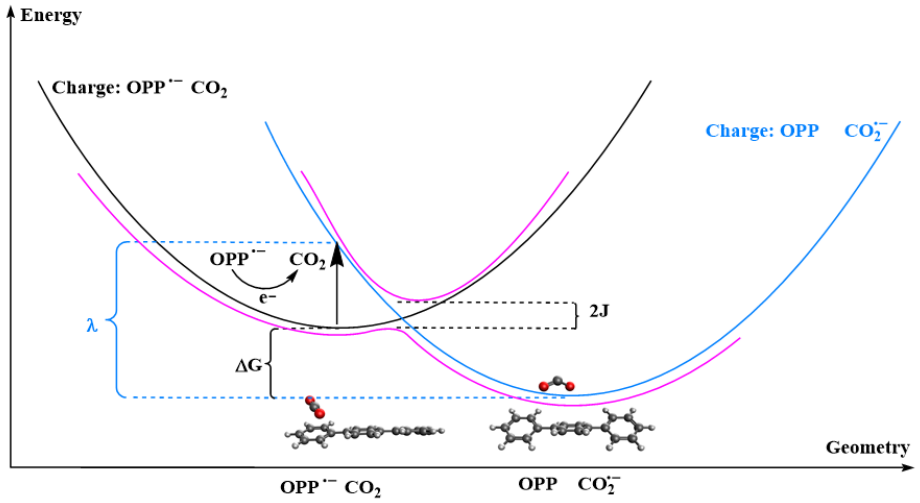

Figure 2: A qualitative energy vs. reaction coordinate representation for the ET step where the pink curve represents the adiabatic limit arising from strong coupling: The black curve reflects the charge distribution of the initial state (reactant complex) and blue represents that of the final state (product complex). ΔG is the free energy difference between the two states and λ corresponds to the energy of reorganization of solute and solvent.

Figure 2 illustrates geometries of initial and final states. In the initial state, the quenched radical anion, $OPP^{\cdot -}$, exhibits a flattened geometry in agreement with prior studies.[17] In the

presence of bent $CO_2^{\cdot -}$ in the final state, substituted OPP adopts either an alternating structure, wherein phenyl rings exhibit alternating tilts, or a helical structure in which each phenyl ring is twisted relative to its predecessor.[20,23,50] These structures are typically different from isolated, ground state OPP geometries. However, the two ground state configurations are very similar in energy (Table 3, SI) and exhibit negligible differences in excitation energies. Therefore, lowest energy conformers for each state are taken into account while reporting excitation energies and ET kinetics. In addition, the configuration of CO_2 depicted in the reactant shown in Figure 2 is one of two possible arrangements of CO_2 with respect to terphenyl. For some substituents, a second minimum is identified where CO_2 resides over the central phenyl. Although these minima cannot be determined for all systems, their energies are very similar to the off-center reactants (Table 4, SI). Therefore, we utilize the off-center structures for all substituents. ΔG is calculated as the energy difference between final and initial states, and λ as the difference between the VCT and final states.[51] λ is calculated using the Q-Chem implementation of the state-specific model for non-equilibrium solvation.[52–56] Table 5 of SI shows, through a limited analysis of functional dependence, that λ values are not significantly affected by the choice of level of theory. Both ΔG and λ are approximated as electronic energies. This is because thermochemical corrections cannot be reliably estimated for the VCT geometries owing to the presence of several imaginary frequencies in their vibrational spectra. These imaginary frequencies are not observed for the product or the reactant state. However, the implicit solvation model ensures that free energies of solvation are accurately represented.

The second generation absolutely localized molecular orbital-EDA (ALMO-EDA)[34,57–61] is employed to characterize electronic interactions between the catalyst and CO_2 in the initial, final, and VCT states. EDA describes electronic interactions (E_{INT}) between two fragments by breaking them into their constituents:

$$E_{INT} = E_{PRP} + E_{FRZ} + E_{POL} + E_{CT} \tag{4}$$

E_{PRP} is the energy required to prepare the two fragment geometries separately. E_{FRZ}, is the energy difference between the sum of isolated fragments' energies and energies of fragments when they are brought to their equilibrium separation without electronic relaxation. Frozen interactions are further broken down into electrostatics, Pauli repulsions, and dispersion:

$$E_{FRZ} = E_{ELEC} + E_{PAULI} + E_{DISP} \tag{5}$$

After the two fragments are brought together, they are allowed to polarize each other without any inter-fragment mixing. This polarization energy is denoted as E_{POL}. The final term, E_{CT}, corresponds to inter-fragment mixing and relaxation, or charge transfer. Since EDA that includes solvation effects is currently still under development in Q-Chem, interfragment interactions are calculated in the gas phase. We expect that inclusion of solvent effects in EDA will lead to stabilization of excess charge and therefore lead to a reduction in electrostatic contributions compared to the gas phase. However, our main focus is on how these interactions vary with OPP substituents. The impact of solvation on these trends is expected to be small. Moreover, given the large size of OPP, we believe its charge distribution will be only modestly affected by the absence of solvent.

Results and Discussion

For the twenty systems chosen in this study, we analyze the impact of substituent electrophilicity, characterized by the para-substituted Hammett parameter (σ_p),[62,63] on all terms constituting the Marcus rate expression as well as the resulting trends in rate coefficients. All results are reported in Table 6 of SI.

Free energy: ΔG

Figure 3 depicts variations in ΔG, λ, and resulting ΔG^* (Equation 3) as a function of σ_p for ET across all substituted OPP systems. The driving force, ΔG (Figure 3(A)), becomes

more favorable with decreasing σ_p, which is intuitive since increased electron-donating ability of substituents enhances the reduction potential of $OPP^{\cdot -}$. However, ΔG plateaus for electron-donating substituents with σ_p lower than -0.75. As a result, it is not immediately apparent whether its dependence on σ_p is linear. Since the coefficient of determination, R^2, only increases with increasing number of fitting parameters, R^2 is not a suitable indicator for model selection. Instead, we utilize the modified Akiake Information Criterion (AICc) to identify whether trends in ΔG are linear, quadratic, or higher order with respect to σ_p.[64] A quadratic model with respect to σ_p emerges as the optimal trade-off between model simplicity and goodness of fit. All fitting curves reported in our analysis correspond to models determined using AICc.

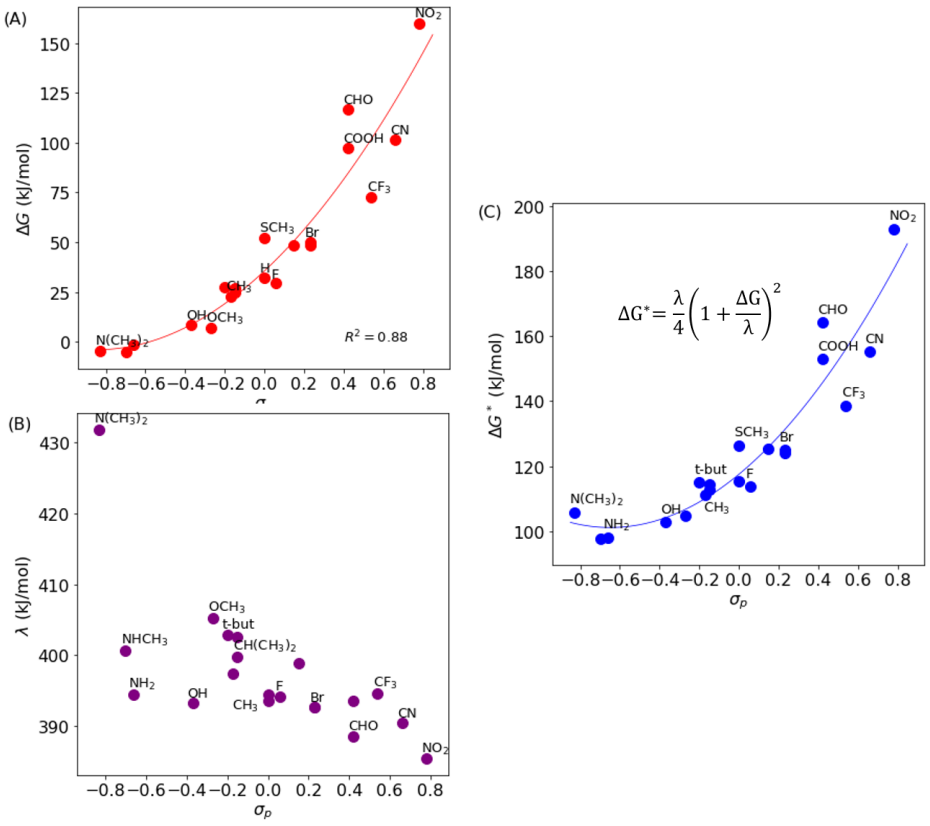

Figure 3: Trends in (A) ΔG ($R^2 = 0.90$), (B) λ, and (C) ΔG^* ($R^2 = 0.88$), plotted vs. Hammett parameter, σ_p. From left to right in each plot, electron-withdrawing ability of the substituent increases. Trendlines to fit the data are determined using the AICc criterion.[64]

To identify the origins of this quadratic dependence, we examine the molecular orbitals

of $OPP^{\cdot -}$. For all substituted OPPs, trends in the highest singly occupied molecular orbital (SOMO) energy of the radical anion $OPP^{\cdot -}$ closely follow LUMO energies of the corresponding neutral OPP. Therefore, we utilize DFT to calculate the HOMO and LUMO levels of substituted, neutral OPPs. While we are aware that HOMO-LUMO gaps are typically underestimated with DFT,[65] our goal is to uncover substituent dependence of LUMO rather than calculate these gaps accurately. The results, reported in Figure 4, show variation in HOMO and LUMO energies with σ_p and the quadratic fitting curves determined using AICc.

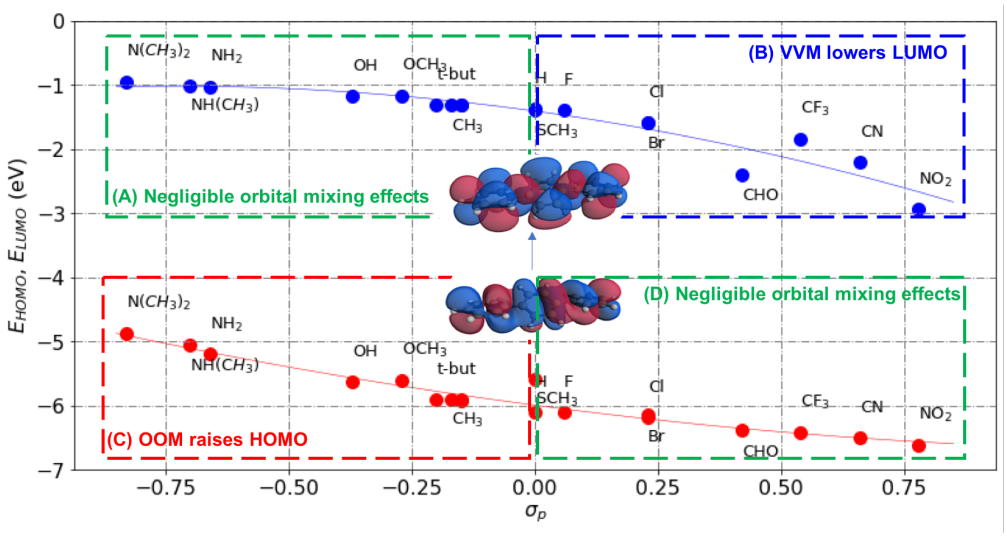

Figure 4: HOMO (red) and LUMO (blue) energies (eV) vs. σ_p for substituted OPPs. Inset: canonical molecular HOMO and LUMO for unsubstituted OPP. Trendlines, based on AICc, reflect quadratic dependence on σ_p ($R^2_{HOMO} = 0.94, R^2_{LUMO} = 0.90$). A qualitative depiction of regions of varying extents of orbital mixing is also shown. The boxes shown here are qualitative pending future analysis with variational EDA.

The linear regions of HOMO and LUMO curves in Figure 4 are straightforward to interpret. Electron-donating groups make it easier to remove an electron from the molecule or, in other words, lower the ionization potential by raising HOMO. Conversely, electron-withdrawing groups make it easier to accept an electron by lowering LUMO levels. To understand the plateaus in LUMO and HOMO levels for strongly electron-donating and withdrawing groups, respectively, we turn to a recent study by Mao and coworkers.[66] The authors adapt a variational EDA procedure to quantify the impact of substituents on photophysical properties of naphthalene. The CT component of EDA between substituent and naphthalene

is broken down into constituent occupied-occupied, virtual-virtual, and occupied-virtual mixing (OOM, VVM, and OVM, respectively) of the fragment orbitals. They observe that OOM between substituent and parent molecule is stronger for electron-donating groups (specifically $N(CH_3)_2$, the strongest donor in this study) leading to an elevated HOMO energy, while VVM is stronger for electron-withdrawing groups leading to a lower LUMO energy. As shown above in Figure 4 in boxes B and C, we observed a similar increase in HOMO levels for electron-donating groups and LUMO levels for electron-withdrawing groups, respectively.

Mao and coworkers also find that VVM contributes negligibly to LUMO levels for strongly electron-donating groups in the same way that OOM does not significantly shift HOMO levels for electron-withdrawing groups – represented by boxes A and D in Figure 4. The final type of mixing, OVM, counteracts the dominant shifts observed for electron-donating groups and electron-withdrawing groups, but the authors observe OOM (VVM) is larger than OVM for strongly electron-donating (withdrawing) groups. LUMO trends in between these extremes are the consequence of trade-offs between VVM and OVM. While a detailed analysis of excited states of substituted OPPs using variational EDA constitutes future work, we believe that the trends we see here are similar, and that plateauing LUMO in Figure 4 is a consequence of decreasing VVM with increasing electron-donating character. Consequently SOMO levels of $OPP^{\cdot -}$ also plateau (Table 7, SI), leading to smaller changes in driving force, ΔG, despite the increase in electron-donating ability of substituents.

To characterize the nature of binding between $OPP^{\cdot -}$ (OPP) and CO_2 ($CO_2^{\cdot -}$), we decompose interactions between the catalyst and substrate fragments in the initial and final states that define ΔG (Table 8, SI). For the initial states, total interaction energies as well as their constituent terms are similar across all systems and so their deviation from unsubstituted OPP is small. EDA results depicted in Figure 5 largely reflect interfragment interaction differences in the final state. In the absence of solvation, electrostatics and charge transfer dominate differences in catalyst-substrate interactions between substituents. $\Delta\Delta E_{ELEC}$ is more negative for electron-withdrawing groups on OPP since they serve to stabilize the an-

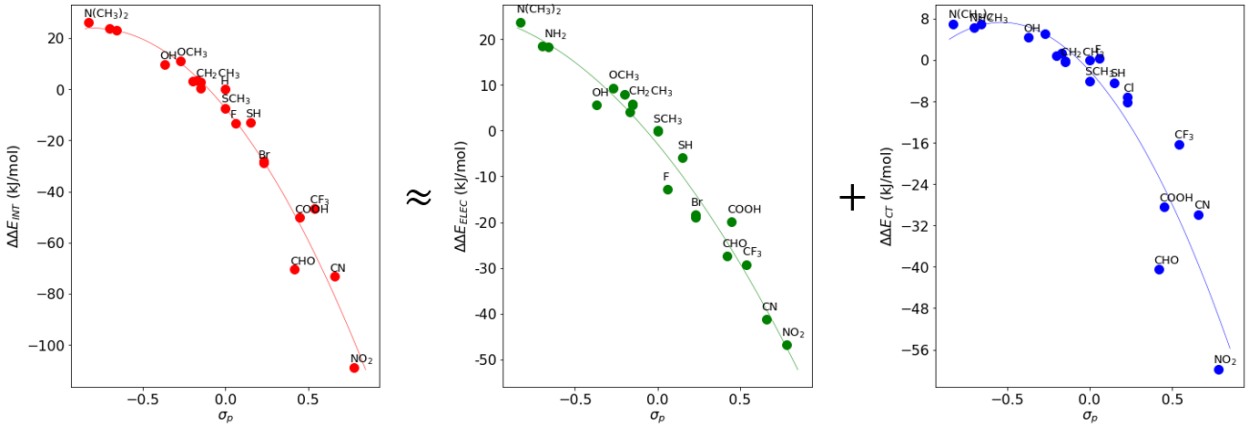

Figure 5: Gas phase EDA results describing differences in interfragment interaction energies between final and initial states relative to the interaction energies of unsubstituted OPP: $\Delta\Delta E_{INT}$ (left, $R^2 = 0.96$) and its main contributors, $\Delta\Delta E_{ELEC}$ (middle, $R^2 = 0.97$) and $\Delta\Delta E_{CT}$ (right, $R^2 = 0.86$). Both electrostatic and charge transfer interactions in the final state are more favorable for electron-withdrawing groups.

ionic $CO_2^{\cdot -}$. Interfragment orbital relaxation is also more favorable for electron-withdrawing groups in the final state, as a result of which $\Delta\Delta E_{CT}$ decreases with increasing σ_p. The strong decrease in $\Delta\Delta E_{CT}$ from left to right is in line with the LUMO level shifts observed for electron-withdrawing groups but not donating groups in Figure 4.

Therefore, while a very wide range of ΔG is observed upon varying σ_p, plateauing LUMO levels limit driving forces achievable with strong electron-donating groups. EDA shows that, in addition to decreasing ΔG, electron-donating groups destabilize the final state and therefore lower the likelihood of occurrence of the reverse reaction. Though the interactions are calculated in the gas phase in the absence of solvent effects, we expect overall trends to be similar in the presence of solvent, with a reduction in magnitude of electrostatic terms due to dielectric screening.

Reorganization energy: λ

Figure 3 shows that λ, described as the energy difference between VCT and final state geometries, shows little dependence on electrophilicity. With the exception of $N(CH_3)_2$, reorganization energies lie in a narrower range (385–405 kJ/mol) compared to ΔG, with little

impact on trends in ΔG^* or rate coefficients. Since λ represents the free energy change associated with structural rearrangement of the solutes and solvent after ET, a closer examination of key changes to the solvated complex geometry is necessary. The bending of solvated CO_2 to accommodate the additional electron in the product state contributes about 270 kJ/mol to the overall reorganization energy based on isolated CO_2 calculations.

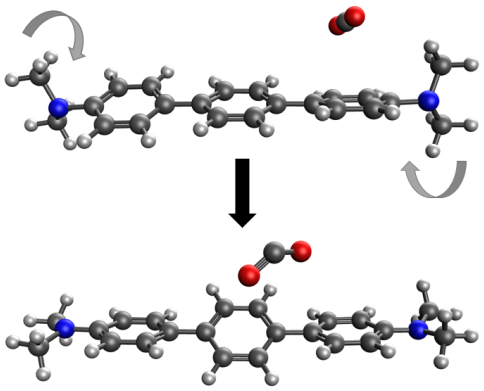

Figure 6: Torsional rotation of the substituent relative to terphenyl in the VCT (top) and final state (bottom) for the $N(CH_3)_2$–substituted system.

Inner sphere reorganization of the catalyst can be broken down into contributions from terphenyl and the substituent. Though the phenyl rings undergo torsional changes after ET, these changes are similar across all substituted terphenyls and do not contribute to differences in reorganization energies. Figure 6 shows the torsional rotation of the substituent when the VCT geometry undergoes relaxation to the final state. For substituents with lone pairs of electrons and methyl groups, relaxation involves rotation of the methyl group from its position perpendicular to the terphenyl plane in the VCT geometry to a position along the plane in the final state. The OPP substituted with $N(CH_3)_2$ undergoes substantial torsional rotation of the substituent (125°) and consequently has a larger reorganization energy. On the other hand, the OPP substituted with NO_2 has the smallest substituent and internal torsional rotations and the smallest reorganization energy.

To further probe substituent effects on the character and extent of interfragment interactions, we use EDA to calculate E_{INT} differences between VCT and final states in the

gas phase. Total energies and dominant components are shown in Figure 7 (Table 9, SI). $\Delta\Delta E_{CT}$ dominates $\Delta\Delta E_{INT}$ because stabilization of the additional electron on linear CO_2 in the VCT state is made possible primarily by interfragment orbital relaxation. Unlike overall reorganization energies, CT contributions depend strongly on substituent electrophilicity. $\Delta\Delta E_{CT}$ is more negative for electron-withdrawing groups since they favor relaxation by pulling electron density away from the center of OPP, thereby accommodating the additional electron on CO_2. This stabilization is partially offset by $\Delta\Delta E_{ELEC}$. Figure 5 and 7 together show that while electron-withdrawing groups lead to favorable electrostatic interactions in the final state, electron-donating groups render interactions in the VCT state less repulsive compared to the final state.

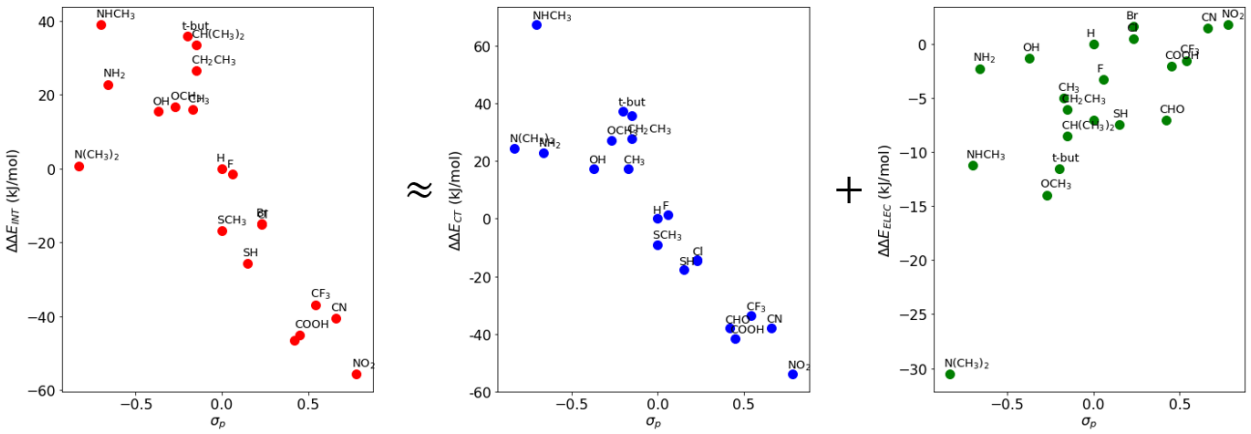

Figure 7: Gas phase EDA results describing differences in interfragment interaction energies between VCT and final states relative to the interaction energies of unsubstituted OPP: $\Delta\Delta E_{INT}$ (left) and its main contributors, $\Delta\Delta E_{CT}$ (middle) and $\Delta\Delta E_{ELEC}$ (right). While charge transfer interactions in VCT are more favorable for electron-withdrawing groups, electrostatics exhibit opposite trends.

We propose a qualitative explanation for the counterintuitive increase in electrostatic stabilization with electron-donating groups, shown in Figure 7, based on electrostatic potential (ESP) maps of the VCT geometries for three representative systems – $NHCH_3$, H, and NO_2. This analysis is along similar lines to molecular quadrupole arguments proposed in the literature for interpreting $\pi-\pi$ and anion-π interactions.[67] ESP maps are shown in Figure 8. With electron-donating groups, a partial positive charge is created at the substituent, which

interacts favorably with the negatively charged substrate fragment in the VCT state. With increasing electron-withdrawing character, the substituent assumes a net negative charge, which repels the negative charge on $CO_2^{\cdot -}$, leading to more repulsive electrostatic interactions seen in Figure 7. Along similar lines, quadrupole interactions in the initial state are hypothesized as the reason behind the off-center orientation of CO_2 over $OPP^{\cdot -}$. However, we anticipate these electrostatic effects will be damped upon inclusion of solvation contributions in EDA. Therefore, charge transfer contributions dominate interfragment interaction differences between VCT and final states.

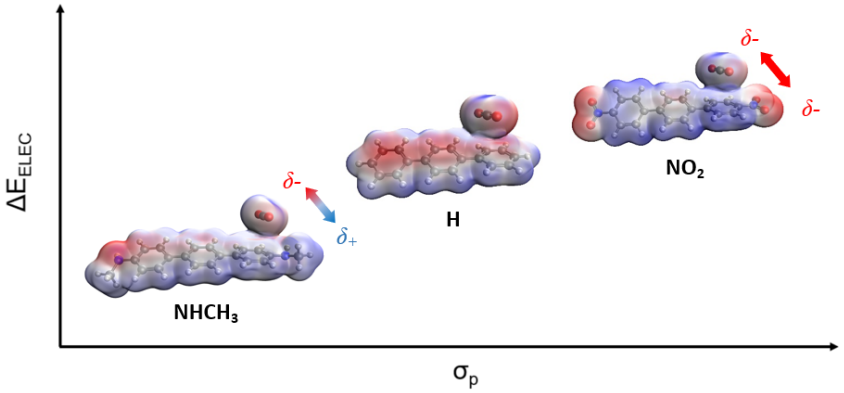

Figure 8: Electrostatic potential maps of the VCT state for $NHCH_3$, H, and NO_2-substituted OPPs. Increasing electron-withdrawing character of the substituent introduces repulsive interactions between partial negative charges in the $CO_2^{\cdot -}$ and electron-rich substituents.

Therefore, even though interfragment interactions constituting λ depend on substituent electrophilicity, their overall contribution to λ are smaller than structural and solvent relaxations. As a result, reorganization energies do not exhibit direct dependence on σ_p.

Free energy of activation: ΔG^*

As illustrated in Figure 3, trends in ΔG^* are largely determined by ΔG for substituted OPPs. Since the latter shows only weakly quadratic dependence on σ_p, AICc identifies a quadratic (rather than quartic) model as the best fit for ΔG^*. The barriers are highest for strongly electron-withdrawing groups and decrease with increasing electron-donating character. For

the most electron-donating system, however, a combination of flattening ΔG and increase in λ leads to a net increase in ΔG^*. As a result, the minimum barrier is obtained, not for the most electron-donating $N(CH_3)_2$, but for the $NHCH_3$-substituted OPP.

Charge transfer integral: J

The diabatic couplings are all in the range of 295-615 meV, which indicates that the electron transfer occurs in the adiabatic regime.[49] That this reaction lies in the adiabatic ET regime was previously unreported and indicates that overall rate coefficients are predominantly influenced by the exponential term across all substituents. However, we still explore the role of substituent in tuning diabatic couplings described by the charge transfer integral, J. While electron-donating groups lower the diabatic couplings relative to H-substituted OPP, electron-withdrawing groups lead to small enhancements in J (Table 2, SI). Although J is known to be a strong function of interfragment separation,[30,68,69] combined changes in substituents and interfragment separations make it difficult to isolate the role played by σ_p in determining J. If this reaction were in the nonadiabatic regime, the small couplings for electron-donating groups could lead to decreased rates, but the magnitudes of J observed in our work indicate that couplings are not quenching ET rate coefficients.

Finally, we note that the large coupling values that we obtain would lead to adiabatic splittings that would lower the estimated Marcus theory activation energy by several tenths of an eV. We do not include this effect in our calculation of the activation energy or rate since the diabatic couplings are similar across the series and, were the geometries thermally averaged, the activation energies would likely be less impacted. Were the energy lowering due to coupling included, there would be little impact on the conclusions we draw here.

ET rate coefficients: k

Since the exponential ΔG^* term determines the rate coefficient, trends in $ln(k)$ reflect ΔG^*, with a quadratic dependence on σ_p observed in Figure 9. The k values shown in Table 6

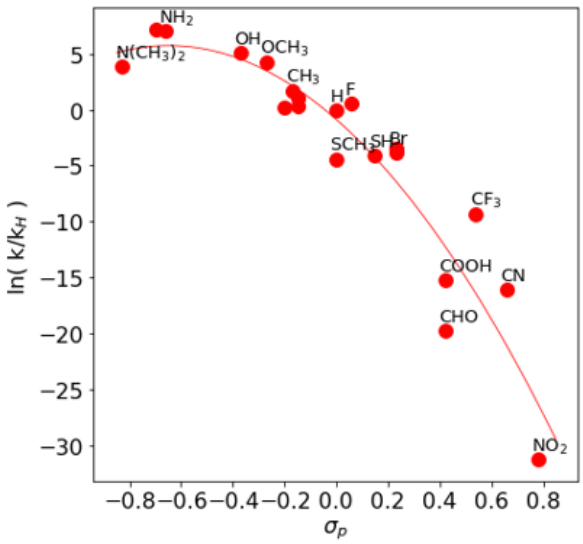

Figure 9: Variation of natural logarithm of the ET rate coefficients, referenced to unsubstituted OPP, ln(k/k$_H$) ($R^2 = 0.88$), with respect to σ_p.

of SI are significantly lower than expected even though we are unable to carry out a direct comparison with experiment. For instance, the calculated rate coefficient for unsubstituted OPP (k_H) is $\sim$1e-7s^{-1} while prior experiments report reasonable reaction timescales (minutes to hours).[17] However, since we are only interested in trends with substituent electrophilicity, the sources of uncertainty in calculated rate coefficients are not examined. k values drop rapidly with increasing electron-withdrawing character of the substituents. In the absence of significant changes in reorganization energy, it is expected that $ln(k)$ plateaus with increasing electron-donating character. However, a decrease in $ln(k)$ is observed, which is attributable to the combined impact of flattening ΔG and steep increase in λ for N(CH$_3$)$_2$. Therefore, for the range of substituent electrophilicities examined in this work, rate coefficients exhibit a maximum for NHCH$_3$, and decline with both increasing and decreasing electron-donating character.

Conclusions

The story of electron transfer from organic photoredox catalysts to CO_2 is a complex one. While the excited state properties of OPPs are well-understood, their viability as green photoredox catalysts for sustainable chemistry is underexplored. Prior to this study, it was unknown whether this electron transfer occurred in the weakly-coupled (Marcus) or strongly-coupled (adiabatic) regime. By calculating the diabatic couplings, we demonstrate that this electron transfer occurs in the adiabatic regime with rate coefficient trends directly and exponentially dependent on the reaction barrier. Enhancing ET rates by increasing electron-donating character of substituents is an intuitive way forward for developing active photoredox catalysts. However, this method for tuning electronic properties is based on the assumption that the free energy driving force increases monotonically with increasing electron-donating character and is the dominant contributor to ET rates. We demonstrate here that rate coefficients unexpectedly decrease for the most electron-donating substituents. This is the combined outcome of flattening free energies, caused by a plateau in LUMO levels of OPP, and increasing reorganization energy driven by large catalyst deformations following ET. Therefore, while substituent electrophilicity, σ_p, is used as the independent variable that describes trends in rate coefficients, it is far from being a complete descriptor. In this study, for instance, we note that the presence of lone pairs on the substituent, rather than its electrophilicity, can lead to higher reorganization energies. Therefore, free energy driving forces cannot be increased indefinitely nor can other components, including reorganization energies, assumed to be invariant while screening these organic photoredox catalysts for CO_2 reduction.

This study also presents a first attempt towards characterizing the nature and extent of interfragment interactions underlying free energy changes in these systems. Our novel use of EDA shows the evolution of dominant interfragment interactions – charge transfer and electrostatics – over the course of ET and reorganization. After the electron is transferred instantaneously from terphenyl to CO_2, an VCT state is formed with large, negative charge

transfer interactions that become more favorable with increasing electron-withdrawing character. As the VCT state undergoes nuclear relaxation, the charge transfer interactions decrease rapidly and electrostatic interactions dominate total interaction energies. These electrostatic forces are repulsive for electron-donating groups and attractive for electron-withdrawing groups, indicating that systems with electron-donating groups are less likely to favorably interact and undergo a reverse reaction. Going forward, we aim to employ EDA for solvated systems to probe the impact of solvent on interfragment interactions, to more accurately reflect the experimental conditions under which CO_2 reduction occurs. We will also utilize variational ALMO-EDA to quantify OOM, VVM, and OVM contributions that lead to plateauing of HOMO and LUMO levels for strongly electron-withdrawing and donating groups, respectively.[66] Given the limitations of σ_p as the sole catalyst design parameter, characterization of electronic properties and interfragment interactions using techniques such as EDA will play a critical role in the identification of substituent, chain length, and conformer combinations that constitute viable organic photoredox catalysts for energy-efficient and sustainable CO_2 conversion and utilization.

Acknowledgement

The authors thank Prof. Jahan Dawlaty (USC) and Dr. Yuezhi Mao (Stanford University) for helpful suggestions. KJK acknowledges support from USC's Graduate Fellowship (2018-19) and the Mork Fellowship (2019-20). SMS acknowledges support from USC's startup funds. SJG acknowledges support from the Young Researchers Program at USC. RJC gratefully acknowledges support from the National Science Foundation (CHE-1565743) and Harvey Mudd College. The authors are also grateful to USC's High Performance Computing center for computing resources and technical support.

Supporting Information Available

Supporting information contains Cartesian XYZ coordinates for all initial and final states, as well as additional computational data and experimental references.

References

(1) Cerling, T. E.; Dearing, M. D.; Ehleringer, J. R. *A history of atmospheric CO_2 and its effects on plants, animals, and ecosystems*; Springer, 2005.

(2) Li, K.; An, X.; Park, K. H.; Khraisheh, M.; Tang, J. A critical review of CO_2 photoconversion: Catalysts and reactors. *Catalysis Today* **2014**, *224*, 3–12.

(3) Windle, C. D.; Perutz, R. N. Advances in molecular photocatalytic and electrocatalytic CO2 reduction. *Coordination Chemistry Reviews* **2012**, *256*, 2562–2570.

(4) White, J. L.; Baruch, M. F.; Pander III, J. E.; Hu, Y.; Fortmeyer, I. C.; Park, J. E.; Zhang, T.; Liao, K.; Gu, J.; Yan, Y., et al. Light-driven heterogeneous reduction of carbon dioxide: photocatalysts and photoelectrodes. *Chemical reviews* **2015**, *115*, 12888–12935.

(5) Lian, S.; Kodaimati, M. S.; Dolzhnikov, D. S.; Calzada, R.; Weiss, E. A. Powering a CO_2 reduction catalyst with visible light through multiple sub-picosecond electron transfers from a quantum dot. *Journal of the American Chemical Society* **2017**, *139*, 8931–8938.

(6) Yeung, C. S. Photoredox catalysis as a strategy for CO_2 incorporation: direct access to carboxylic acids from a renewable feedstock. *Angewandte Chemie International Edition* **2019**, *58*, 5492–5502.

(7) Sato, S.; Morikawa, T.; Kajino, T.; Ishitani, O. A highly efficient mononuclear irid-

ium complex photocatalyst for CO_2 reduction under visible light. *Angewandte Chemie International Edition* **2013**, *52*, 988–992.

(8) Moore, J. N.; Luoma, S. N. Hazardous wastes from large-scale metal extraction. A case study. *Environmental Science & Technology* **1990**, *24*, 1278–1285.

(9) Tchounwou, P. B.; Yedjou, C. G.; Patlolla, A. K.; Sutton, D. J. *Molecular, Clinical and Environmental Toxicology*; Springer, 2012; pp 133–164.

(10) Romero, N. A.; Nicewicz, D. A. Organic photoredox catalysis. *Chemical Reviews* **2016**, *116*, 10075–10166.

(11) McCarthy, B. G.; Pearson, R. M.; Lim, C.-H.; Sartor, S. M.; Damrauer, N. H.; Miyake, G. M. Structure–property relationships for tailoring phenoxazines as reducing photoredox catalysts. *Journal of the American Chemical Society* **2018**, *140*, 5088–5101.

(12) Sprick, R. S.; Jiang, J.-X.; Bonillo, B.; Ren, S.; Ratvijitvech, T.; Guiglion, P.; Zwijnenburg, M. A.; Adams, D. J.; Cooper, A. I. Tunable organic photocatalysts for visible-light-driven hydrogen evolution. *Journal of the American Chemical Society* **2015**, *137*, 3265–3270.

(13) Shaw, M. H.; Twilton, J.; MacMillan, D. W. Photoredox catalysis in organic chemistry. *The Journal of Organic Chemistry* **2016**, *81*, 6898–6926.

(14) Prier, C. K.; Rankic, D. A.; MacMillan, D. W. Visible light photoredox catalysis with transition metal complexes: applications in organic synthesis. *Chemical Reviews* **2013**, *113*, 5322–5363.

(15) Xuan, J.; Xiao, W.-J. Visible-light photoredox catalysis. *Angewandte Chemie International Edition* **2012**, *51*, 6828–6838.

(16) Du, Y.; Pearson, R. M.; Lim, C.-H.; Sartor, S. M.; Ryan, M. D.; Yang, H.; Damrauer, N. H.; Miyake, G. M. Strongly reducing, visible-light organic photoredox cat-

alysts as sustainable alternatives to precious metals. *Chemistry–A European Journal* **2017**, *23*, 10962–10968.

(17) Matsuoka, S.; Kohzuki, T.; Pac, C.; Ishida, A.; Takamuku, S.; Kusaba, M.; Nakashima, N.; Yanagida, S. Photocatalysis of oligo (p-phenylenes): photochemical reduction of carbon dioxide with triethylamine. *The Journal of Physical Chemistry* **1992**, *96*, 4437–4442.

(18) Seo, H.; Katcher, M. H.; Jamison, T. F. Photoredox activation of carbon dioxide for amino acid synthesis in continuous flow. *Nature Chemistry* **2017**, *9*, 453.

(19) Seo, H.; Liu, A.; Jamison, T. F. Direct β-selective hydrocarboxylation of styrenes with CO2 enabled by continuous flow photoredox catalysis. *Journal of the American Chemical Society* **2017**, *139*, 13969–13972.

(20) Guiglion, P.; Zwijnenburg, M. A. Contrasting the optical properties of the different isomers of oligophenylene. *Physical Chemistry Chemical Physics* **2015**, *17*, 17854–17863.

(21) Ma, J.; Li, S.; Jiang, Y. A time-dependent DFT study on band gaps and effective conjugation lengths of polyacetylene, polyphenylene, polypentafulvene, polycyclopentadiene, polypyrrole, polyfuran, polysilole, polyphosphole, and polythiophene. *Macromolecules* **2002**, *35*, 1109–1115.

(22) Ivanov, M. V.; Talipov, M. R.; Boddeda, A.; Abdelwahed, S. H.; Rathore, R. Hückel Theory+ Reorganization Energy= Marcus–Hush Theory: Breakdown of the 1/n Trend in π-Conjugated Poly-p-phenylene Cation Radicals Is Explained. *The Journal of Physical Chemistry C* **2017**, *121*, 1552–1561.

(23) Lukeš, V.; Aquino, A. J. A.; Lischka, H.; Kauffmann, H.-F. Dependence of optical properties of oligo-para-phenylenes on torsional modes and chain length. *The Journal of Physical Chemistry B* **2007**, *111*, 7954–7962.

(24) Hartley, C. S. Excited-state behavior of ortho-phenylenes. *The Journal of Organic Chemistry* **2011**, *76*, 9188–9191.

(25) Koch, R.; Finnerty, J. J.; Bruhn, T. Theoretical study on the nonlinear optical properties of phenylenes and influencing factors. *Journal of Physical Organic Chemistry* **2008**, *21*, 954–962.

(26) He, J.; Crase, J. L.; Wadumethrige, S. H.; Thakur, K.; Dai, L.; Zou, S.; Rathore, R.; Hartley, C. S. ortho-Phenylenes: Unusual conjugated oligomers with a surprisingly long effective conjugation length. *Journal of the American Chemical Society* **2010**, *132*, 13848–13857.

(27) Wenger, O. S. Photoinduced electron and energy transfer in phenylene oligomers. *Chemical Society Reviews* **2011**, *40*, 3538–3550.

(28) Panda, A. N.; Plasser, F.; Aquino, A. J.; Burghardt, I.; Lischka, H. Electronically excited states in poly (p-phenylenevinylene): Vertical excitations and torsional potentials from high-level Ab initio calculations. *The Journal of Physical Chemistry A* **2013**, *117*, 2181–2189.

(29) Yan, L.; Zhao, Y.; Yu, H.; Hu, Z.; He, Y.; Li, A.; Goto, O.; Yan, C.; Chen, T.; Chen, R., et al. Influence of heteroatoms on the charge mobility of anthracene derivatives. *Journal of Materials Chemistry C* **2016**, *4*, 3517–3522.

(30) Ottonelli, M.; Duce, D.; Thea, S.; Dellepiane, G. The Influence of the Vinyl Terminal Group on the Poly (Para-Phenylenevinylene) Charge Transfer Integrals. *Journal of Nanoscience and Nanotechnology* **2013**, *13*, 5186–5193.

(31) Wada, Y.; Kitamura, T.; Yanagida, S. CO_2-fixation into organic carbonyl compounds in visible-light-induced photocatalysis of linear aromatic compounds. *Research on Chemical Intermediates* **2000**, *26*, 153–159.

(32) Liu, R.; Yang, L.; Yang, T.; Huang, Y.; Barbatti, M.; Jiang, J.; Zhang, G. Modulating Electron Transfer in an Organic Reaction via Chemical Group Modification of the Photocatalyst. *The Journal of Physical Chemistry Letters* **2019**, *10*, 5634–5639.

(33) Wu, Q.; Van Voorhis, T. Constrained density functional theory and its application in long-range electron transfer. *Journal of Chemical Theory and Computation* **2006**, *2*, 765–774.

(34) Khaliullin, R. Z.; Cobar, E. A.; Lochan, R. C.; Bell, A. T.; Head-Gordon, M. Unravelling the Origin of Intermolecular Interactions Using Absolutely Localized Molecular Orbitals. *The Journal of Physical Chemistry A* **2007**, *111*, 8753–8765.

(35) Hohenberg, P.; Kohn, W. Inhomogeneous electron gas. *Physical Review* **1964**, *136*, B864.

(36) Kohn, W.; Sham, L. J. Self-consistent equations including exchange and correlation effects. *Physical Review* **1965**, *140*, A1133–A1138.

(37) Shao, Y. et al. Advances in molecular quantum chemistry contained in the Q-Chem 4 program package. *Molecular Physics* **2015**, *113*, 184–215.

(38) Becke, A. D. Density-functional thermochemistry. III. The role of exact exchange. *The Journal of Chemical Physics* **1993**, *98*, 5648–5652.

(39) Truong, T. N.; Stefanovich, E. V. A new method for incorporating solvent effect into the classical, ab initio molecular orbital and density functional theory frameworks for arbitrary shape cavity. *Chemical Physics Letters* **1995**, *240*, 253 – 260.

(40) Barone, V.; Cossi, M. Quantum Calculation of Molecular Energies and Energy Gradients in Solution by a Conductor Solvent Model. *The Journal of Physical Chemistry A* **1998**, *102*, 1995–2001.

(41) Cossi, M.; Rega, N.; Scalmani, G.; Barone, V. Energies, structures, and electronic properties of molecules in solution with the C-PCM solvation model. *Journal of Computational Chemistry 24*, 669–681.

(42) Grimme, S.; Ehrlich, S.; Goerigk, L. Effect of the damping function in dispersion corrected density functional theory. *Journal of Computational Chemistry* **2011**, *32*, 1456–1465.

(43) Johnson, E. R.; Becke, A. D. A post-Hartree-Fock model of intermolecular interactions: Inclusion of higher-order corrections. *The Journal of Chemical Physics* **2006**, *124*, 174104.

(44) Casida, M. E. *Recent Advances In Density Functional Methods: (Part I)*; World Scientific, 1995; pp 155–192.

(45) Dreuw, A.; Head-Gordon, M. Single-reference ab initio methods for the calculation of excited states of large molecules. *Chemical Reviews* **2005**, *105*, 4009–4037.

(46) Banerjee, M.; Shukla, R.; Rathore, R. Synthesis, optical, and electronic properties of soluble poly-p-phenylene oligomers as models for molecular wires. *Journal of the American Chemical Society* **2009**, *131*, 1780–1786.

(47) Marcus, R. A. On the theory of oxidation-reduction reactions involving electron transfer. I. *The Journal of Chemical Physics* **1956**, *24*, 966–978.

(48) Wu, Q.; Van Voorhis, T. Extracting electron transfer coupling elements from constrained density functional theory. *The Journal of Chemical Physics* **2006**, *125*, 164105.

(49) Brunschwig, B. S.; Logan, J.; Newton, M. D.; Sutin, N. A semiclassical treatment of electron-exchange reactions. Application to the hexaaquoiron (II)-hexaaquoiron (III) system. *Journal of the American Chemical Society* **1980**, *102*, 5798–5809.

(50) Lukeš, V.; Šolc, R.; Barbatti, M.; Elstner, M.; Lischka, H.; Kauffmann, H.-F. Torsional potentials and full-dimensional simulation of electronic absorption and fluorescence spectra of para-phenylene oligomers using the semiempirical self-consistent charge density-functional tight binding approach. *The Journal of Chemical Physics* **2008**, *129*, 164905.

(51) Wu, Q.; Van Voorhis, T. Direct calculation of electron transfer parameters through constrained density functional theory. *The Journal of Physical Chemistry A* **2006**, *110*, 9212–9218.

(52) Cammi, R.; Tomasi, J. Nonequilibrium solvation theory for the polarizable continuum model: A new formulation at the SCF level with application to the case of the frequency-dependent linear electric response function. *International Journal of Quantum Chemistry* **1995**, *56*, 465–474.

(53) Cossi, M.; Barone, V. Separation between fast and slow polarizations in continuum solvation models. *The Journal of Physical Chemistry A* **2000**, *104*, 10614–10622.

(54) Improta, R.; Barone, V.; Scalmani, G.; Frisch, M. J. A state-specific polarizable continuum model time dependent density functional theory method for excited state calculations in solution. *The Journal of Chemical Physics* **2006**, *125*, 054103.

(55) You, Z.-Q.; Mewes, J.-M.; Dreuw, A.; Herbert, J. M. Comparison of the Marcus and Pekar partitions in the context of non-equilibrium, polarizable-continuum solvation models. *The Journal of chemical physics* **2015**, *143*, 204104.

(56) Mewes, J.-M.; You, Z.-Q.; Wormit, M.; Kriesche, T.; Herbert, J. M.; Dreuw, A. Experimental benchmark data and systematic evaluation of two a posteriori, polarizable-continuum corrections for vertical excitation energies in solution. *The Journal of Physical Chemistry A* **2015**, *119*, 5446–5464.

(57) Horn, P. R.; Sundstrom, E. J.; Baker, T. A.; Head-Gordon, M. Unrestricted absolutely localized molecular orbitals for energy decomposition analysis: Theory and applications to intermolecular interactions involving radicals. *The Journal of Chemical Physics* **2013**, *138*, 134119.

(58) Horn, P. R.; Head-Gordon, M. Polarization contributions to intermolecular interactions revisited with fragment electric-field response functions. *The Journal of Chemical Physics* **2015**, *143*, 114111.

(59) Horn, P. R.; Head-Gordon, M. Alternative definitions of the frozen energy in energy decomposition analysis of density functional theory calculations. *The Journal of Chemical Physics* **2016**, *144*, 084118.

(60) Horn, P. R.; Mao, Y.; Head-Gordon, M. Defining the contributions of permanent electrostatics, Pauli repulsion, and dispersion in density functional theory calculations of intermolecular interaction energies. *The Journal of Chemical Physics* **2016**, *144*, 114107.

(61) Horn, P. R.; Mao, Y.; Head-Gordon, M. Probing non-covalent interactions with a second generation energy decomposition analysis using absolutely localized molecular orbitals. *Physical Chemistry Chemical Physics* **2016**, *18*, 23067–23079.

(62) Hammett, L. P. The effect of structure upon the reactions of organic compounds. Benzene derivatives. *Journal of the American Chemical Society* **1937**, *59*, 96–103.

(63) Hansch, C.; Leo, A.; Taft, R. W. A survey of Hammett substituent constants and resonance and field parameters. *Chemical Reviews* **1991**, *91*, 165–195.

(64) Burnham, K. P.; Anderson, D. R. *Model Selection and Multimodel Inference*, 2nd ed.; Springer: New York, NY, 2002.

(65) Refaely-Abramson, S.; Baer, R.; Kronik, L. Fundamental and excitation gaps in

molecules of relevance for organic photovoltaics from an optimally tuned range-separated hybrid functional. *Physical Review B* **2011**, *84*, 075144.

(66) Mao, Y.; Head-Gordon, M.; Shao, Y. Unraveling substituent effects on frontier orbitals of conjugated molecules using an absolutely localized molecular orbital based analysis. *Chemical Science* **2018**, *9*, 8598–8607.

(67) Neel, A. J.; Hilton, M. J.; Sigman, M. S.; Toste, F. D. Exploiting non-covalent π interactions for catalyst design. *Nature* **2017**, *543*, 637–646.

(68) Miller, N. E.; Wander, M. C.; Cave, R. J. A theoretical study of the electronic coupling element for electron transfer in water. *The Journal of Physical Chemistry A* **1999**, *103*, 1084–1093.

(69) Kubas, A.; Hoffmann, F.; Heck, A.; Oberhofer, H.; Elstner, M.; Blumberger, J. Electronic couplings for molecular charge transfer: Benchmarking CDFT, FODFT, and FODFTB against high-level ab initio calculations. *The Journal of Chemical Physics* **2014**, *140*, 104105.

Graphical TOC Entry